CYTOMETRY
Journal of Quantitative Cell Science PART A

Improved Flow Cytometric Light Scatter Detection of Submicron-Sized Particles by Reduction of Optical Background Signals

Ger J. A. Arkesteijn,[1,2*] Estefanía Lozano-Andrés,[1] Sten F. W. M. Libregts,[1] Marca H. M. Wauben[1]

[1]Department of Biochemistry and Cell Biology, Faculty of Veterinary Medicine, Utrecht University, Utrecht, The Netherlands

[2]Department of Immunology and Infectious Diseases, Faculty of Veterinary Medicine, Utrecht University, Utrecht, The Netherlands

Received 8 August 2019; Revised 6 April 2020; Accepted 8 April 2020

Grant sponsor: Dutch Technology Foundation STW (Perspectief Program Cancer ID), Grant number14191; Grant sponsor: European Union's Horizon 2020 research and innovation programme (Marie Skłodowska-Curie grant) , Grant number722148

Additional Supporting Information may be found in the online version of this article.

*Correspondence to: Ger J. A. Arkesteijn, Department of Biochemistry and Cell Biology, Faculty of Veterinary Medicine, Utrecht University, Yalelaan 2 (Nieuw Gildestein), 3584 CM Utrecht, The Netherlands
Email: g.j.a.arkesteijn@uu.nl

Estefanía Lozano-Andrés and Sten F. W. M. Libregts contributed equally to this study.

Published online in Wiley Online Library (wileyonlinelibrary.com)

DOI: 10.1002/cyto.a.24036

Abstract

Flow cytometry allows multiparameter analysis on a single-cell basis and is currently the method of choice to rapidly assess heterogeneity of cell populations in suspension. With the research field of extracellular vesicles (EV) rapidly expanding, there is an increased demand to address heterogeneity of EV populations in biological samples. Although flow cytometry would be the ideal technique to do so, the available instruments are in general not equipped to optimally detect the dim light scatter signals generated by submicron-sized particles like EV. Although sideward scatter light and fluorescence are currently used as a threshold signal to identify EV within samples, the forward scatter light (FSC) parameter is often neglected due to the lack of resolution to distinguish EV-related signals from noise. However, after optimization of FSC detection by adjusting the size of the obscuration bar, we recently showed that certain EV-subsets could only be identified based on FSC. This observation made us to further study the possibilities to enhance FSC-detection of submicron-sized particles. By testing differently sized obscuration bars and differently sized pinholes in the focal plane behind the FSC detection lens, we generated a matrix that allowed us to determine which combination resulted in the lowest optical background in terms of numbers of events regarding FSC detection of submicron-sized particles. We found that a combination of an 8-mm obscuration bar and a 200-μm pinhole reduced optical background in a reproducible manner to such extent that it allowed a robust separation of 100-nm polystyrene beads from background signals within the FSC channel, and even allowed thresholding on FSC without the interference of massive background signals when both beads and EV were measured. These technical adaptations thus significantly improved FSC detection of submicron-sized particles and provide an important lead for the further development and design of flow cytometers that aid in detection of submicron-sized particles. © 2020 The Authors. *Cytometry Part A* published by Wiley Periodicals, Inc. on behalf of International Society for Advancement of Cytometry.

Key terms

extracellular vesicle; exosome; microvesicle; optical background; light scatter; flow cytometry

FLOW cytometry has become an indispensable tool in biological research. Besides multiparameter analysis of cells in biological samples, flow cytometry is widely used to sort and purify subsets of cells from a heterogeneous population at high speed based on single-cell characteristics. For decades, the design of flow cytometers fulfilled the demands to process cells or cell-sized particles. In recent years, however, there is an increasing demand to process and analyze submicron-sized particles, not least driven by the rapidly expanding research field of extracellular vesicles (EV). It has become evident that EV play crucial roles in many biological processes and bear great potential for biomarker analysis (1). For characterization of EV, flow cytometry

is one of the methods of choice due to the fact that samples can be measured quantitatively and qualitatively with high speed on a single-particle basis. However, considerations have to be taken into account and requirements have to be met before this can be achieved (2). One is the choice of the threshold signal. Historically, the threshold signal used to measure cells is one of the light scatter parameter. All cells and particles scatter light upon interrogation with a laser and thereby produce signals of sufficient strength for detection by even the simplest photodiodes. Therefore, all cells will be "seen" by the flow cytometer and detected as events. Differentiation between cell types, their subset, and other particles can then take place based on the other parameters taken along in the measurement.

Considering the fact that the strength of the light scatter signals is highly dependent on size and refractive index of the particles that are being analyzed, the shortcomings of current flow cytometers regarding light scatter detection quickly become evident for submicron-sized particles like EV, of which the vast majority is smaller than 500 nm (3–6). When measurements rely on light scatter detection, sideward scatter light (SSC) is the preferred parameter of choice since position of the collection lens perpendicular to the laser direction results in significantly lower laser light background. For the measurement of submicron-sized particles the light scatter signals have to be markedly amplified. Increasing the intensity of the laser at the interrogation point is one step in improving strength of dim signals. This could be accomplished by either increasing laser power, applying optical components to decrease the beam waist at the interrogation point, or a combination of both. Increasing laser power will go hand in hand with increased background signals, thereby negatively impacting the detection of light scatter signals of interest. On top of that, increasing illumination intensities cannot be limitlessly applied in cases where fluorescence (FL) comes into play (7). Alternatively, the photomultplier tube (PMT) voltage or gains can be increased to enhance detection, but as such, the optical and electronic background will be prominently amplified as well, thereby hampering the proper read-out of sample specific light scatter signals. To tackle the problem of detection of dim light scatter signals, other threshold parameters with stronger and more specific signals can be deployed. A prerequisite for this is that the signal of the threshold parameter has to be unique and equally strong for all particles that need to be investigated. In the past several approaches have been undertaken to improve the detection of submicron-sized particles, such as prolonging dwell time, application of high resolution optics and differing scatter collection angles (8, 9), resulting in commercially available flow cytometers dedicated for small particle detection. Due to the configuration of most commercially available flow cytometers, SSC generally allows for a better signal-to-noise ratio and provides a better alternative than forward scatter light (FSC) to discriminate dim signals above background (10). We have, however, realized the importance of FSC signals when analyzing EV populations derived from virus-infected cells, in which virus- and nonvirus-containing EVs could solely be discriminated based on different FSC signals (11). This finding illustrates that FSC signals contain valuable information for EV-subset analysis. Alternatively, fluorescence (FL) could provide selective threshold signals (12). In recent years, we therefore have developed a method to generically stain EV in suspension with a fluorescent dye and use emitted fluorescent light as a threshold signal (13). Along with that, we applied specific hardware adaptations to improve the resolution of the FSC parameter (14). This enabled us to quantitatively and qualitatively analyze EV and to sort subpopulations of EV to high purity (11, 15). Measurements that are performed in this way provide information on all EV that emit fluorescent signals above a set threshold level and implicate that all unstained particles remain undetectable. Although this effectively cleans up the measurement by eliminating all particles without enough FL, we have recently shown that particles that remain undetectable when a FL threshold is performed can have a significant impact on light scatter parameters when they occur in high concentrations (16). Here, we aimed at reduction of optical background signals on FSC detection to be able to obtain more reliable information about the weak FSC signals generated by sub-micron sized particles. Optical background as such is the contribution of all photons reaching the FSC detector that are not related to the direct scattering from the particles in the core of the fluid stream. It could either be derived from ambient light, scatter light from particles in the surrounding sheath fluid, or stray light from the laser. Since laser light freely passes the band pass filter in front of the detector, it is a major component of the optical background in the FSC detector.

This made us pursue to find the most sensitive configuration for FSC detection. Key in improving the detection of dim FSC signals is to reduce signals caused by stray light, while keeping specific light scatter unaffected (17). Since the FSC detector is in a straight line with the optical path of the laser from which FSC signals are derived, direct laser light needs to be blocked to prevent it from reaching the detector. An obscuration bar is therefore placed in front of the FSC detection lens to block out direct laser light, while light scatter from passing particles, which scatter light in all angles, pass above and below the obscuration bar and get focused by the collection lens onto the FSC detector. Although in this way most direct laser light is blocked, there will be a fraction of stray light within the flow chamber, unrelated to any particle passage, which additionally scatters in multiple directions. As the FSC detector is equipped with an optical filter that matches the wavelength of the detecting laser, this additional stray light can reach the FSC detector without restriction. Stray light therefore imposes the adjustment of the threshold on the light scatter parameter to a higher level, thereby restricting the measurement to particles with a higher light scattering power.

We have previously demonstrated that we could improve FSC detection of submicron-sized particles by increasing the laser power in combination with a wider obscuration bar in front of the FSC collections lens (14). Here we present a method to further improve the resolution of the FSC

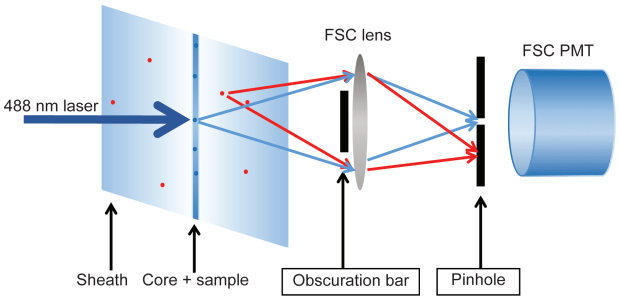

Figure 1. Schematic representation of the optical configuration in front of the FSC detector. With a small pinhole in place, scatter light derived from a confined small area around the core stream only can reach the FSC detector (blue arrows), while light coming in with other angles (either stray light or scatter from occasional particles in the sheath fluid) are blocked (red arrows). The figure does not reflect actual relative sizes and dimensions. [Color figure can be viewed at wileyonlinelibrary.com]

parameter by significantly reducing background light scatter signals during the detection of submicron-sized particles. To configure the flow cytometer, we started off with the small particle detector (SPD) commercially available by BD. The original design held an optical glass plate that had to be placed at Brewster angle. The rationale of the original design of this detector is that polarization direction is altered by small particles depending on size and composition. Both parallel and perpendicular polarization directions can be separated by the Brewster plates and be read as different forward scatter parameters in this SPD. In the past we have extensively studied this but we did not find any discriminatory effect between EV in biological samples. We therefor decided to move away from this principle and actually only use the housing of the detector to build our own SPD. The main effective principle we applied is confocal detection and Figure 1 shows a schematic representation of how the confocal system works in our configuration. For every particle out of the focal spot, the scattering light will be reduced because it is not perfectly focused on the pinhole. Although this figure shows this principle for particles in the sheath, it is applicable for light coming in from any direction that is different than light coming from the focal spot. The aim in this manuscript is to tackle optical background caused by ambient light and laser stray light coming in from any aberrant angle. It has to be considered that such a simplified confocal construction works mainly for nonimaging optical techniques such as flow cytometry. With this in mind we then investigated whether there is an optimal combination for pinhole and blocker bar sizes that aid in reducing the background noise and enhance the signal-to-noise ratio of the FSC-parameter in a reproducible and stable manner.

Materials and Methods

Flow Cytometer Setup

We used a BD Influx Jet in Air sorter that was modified as fully described in van der Vlist et al. (14). FSC was collected with a Plan Apo 20× (NA 0.42) lens (Mitutoyo, Japan). The lens was at near focal distance of the sample core (depending on the adjustment per configuration approximately 19 mm). In front of the objective lens a height adjustable obscuration bar was mounted at a distance of 7 mm to the collection objective. Directly behind the collection objective, a converging 50-mm lens was mounted to focus the light on a pinhole. This pinhole was at 18 mm distance from the glass surface of the PMT. On the basis of this configuration we further experimented with mounting a variety of obscuration bars and pinholes. The sizes of the obscuration bars tested were: 2.5, 3, 5, 8, and 10 mm, whereas the diameters of the tested pinholes were 30, 50, 100, 200, 400, and 700 µm. All obscuration bars were custom made by Becton Dickinson. All pinhole formats were purchased from Thor labs (Newton, NJ), except for the 700-µm pinhole, which was custom made by Becton Dickinson. To observe the relative improvement of FSC detection upon application of the various obscuration bars and pinholes we used 100-nm yellow-green fluorescent (505/515) carboxylate-modified microspheres (FluoSpheres™, ThermoFisher Scientific/Invitrogen, Eugene, F8803, Lot. 1832955) to align the lasers and fluid stream and to normalize each measurement. Trigger signals are taken from the first laser (488 nm). In the analog system of the BD Influx this is also the parameter where the threshold is set on. The term "threshold(ed)" is used throughout the manuscript. For the BD Influx, part of the pulse-processing and related baseline calculations are not sufficiently described, and uncertainty remains about the output value of pulse area. The BD Influx displayed the closest match with other instruments when calibration beads were measured in pulse height mode. Based on this empirical finding, pulse height was used for all measurements in this study. Preamps of the ADC's with a 1.2-µs time constant were used for all of the nontrigger parameters (instead of 0.12 µs, which was used for triggering only).

For normalization of signals, we marked the position of 100-nm fluospheres in a saved workspace containing dot plots with narrow gates and upon swapping obscuration bars or pinholes the system was carefully realigned to reach the highest possible signals (as expressed by the mean fluorescent intensities [MFI]). Thereafter PMT voltages were adjusted such that the 100-nm bead cluster displayed identical MFI and mean light scatter values for each subsequent measurement.

Importantly, to prevent contaminating events to be released from the sample input tube and to clearly visualize the absolute background noise of the flow cytometer and eventual particles residing within the sheath, background measurements were recorded in backflush mode (no sample passing the laser). Next, 100-nm fluospheres were measured and thresholded on either FSC or FL, using the threshold levels indicated in the results section at an event rate of 2000/s. Each sample was run with the same sample (4.29 psi) and sheath (5.0 psi) pressure. Under these conditions the sample core diameter is 6 µm. Calculation of the core diameter was based on the expel of fluid from the nozzle tip (4.56 ml/min) and the sample fluid consumption during a given time period (0.01 ml/min). To calculate the core diameter of the sample,

the total sheath volume per time unit was divided by the volume of the sample during the same time. The following formula was then used (18) to calculate the core diameter:

$$d_c = \sqrt{d_s^2 \times Q}$$

where d_c = core diameter, d_s^2 = stream diameter, and Q = sample volume/total volume.

The pulse length as observed on the digital storage oscilloscope relates to the time the particle dwells in the laser spot. For particles in the submicron range this is 2.5 μs in the described configuration. With the volumetric measurements above we calculated the height of the laser spot to be 13.7 μm and the speed of the particle 5.5 m/s.

Before acquisition, each sample was boosted until events appeared, the stream was then allowed to stabilize for 30 s, after which data were recorded for 30 s using BD Sortware version 1.2.0.142. Data analysis was performed with FlowJo Version 10.5.0 and dot plots presented in this manuscript display ungated data from all events acquired during a 30 s measurement.

Isolation of Cell Culture Supernatant-Derived EV

EV-containing samples were obtained from 4T1 mouse mammary carcinoma cell culture supernatants (ATCC, Manassas, VA) as previously described (19, 20), Briefly, cells were maintained in Dulbecco's minimal essential medium (DMEM) supplemented with 10% fetal calf serum, 100 U/ml penicillin and 100 μg/ml streptomycin (Invitrogen, Carlsbad, CA). To prepare conditioned medium (CM), 4T1 cells were washed once with DMEM, followed by three washing steps with DMEM supplemented with 0.5% EV-depleted fetal bovine serum (EDS). EDS was obtained after 18 h of ultracentrifugation at 100,000*g* and 4°C using a SW55 Ti rotor (Beckman Coulter, Fullerton, CA) and filtered through a 0.22-μm filter (Whatman, Dassel, Germany). Flasks were incubated at 37°C and 5% CO_2 with 15 ml of DMEM containing 0.5% EDS. After 24 h, CM was collected and centrifuged for 10 min at 200*g* and 4°C. Prior to the collection of the CM, cell counting was performed with trypan blue staining to assess cell viability (>90%) by using an automated cell counter (CountessTM, Thermo Fisher Scientific). The supernatant was passed through a 0.45-μm cellulose acetate filter (Corning, NY) and CM was concentrated at 4°C approximately 300 times using a 10-kDa Centricon Plus-70 centrifugal unit (Merck Millipore, Billerica, MA). After filtering through a 0.22-μm filter (Whatman, Dassel, Germany), 1 ml of the concentrated CM (CCM) was used for EV isolation by a combination of Optiprep density-gradient ultracentrifugation and size-exclusion chromatography (SEC), as previously described (19, 20). Briefly, a discontinuous gradient was made by layering 4 ml of 40%, 4 ml of 20%, 4 ml of 10%, and 3.5 ml of 5% iodixanol (Axis-Shield, Oslo, Norway) in a 16.8-ml open top polyallomer tube (Beckman Coulter, Fullerton, CA). One milliliter of CCM was placed on top of the gradient, followed by 18.11 h of ultracentrifugation at 100,000*g* and 4°C using a SW32.1 Ti rotor (Beckman Coulter, Fullerton, CA). Fractions of 1 ml were collected and EV-rich fractions, being 9 and 10, were pooled together. For SEC, Sepharose CL-2B (GE Healthcare, Uppsala, Sweden) was washed three times with phosphate buffered saline (PBS) containing 0.32% trisodiumcitrate dihydrate (ChemCruz, Dallas, TX). For preparation of one column, a nylon net with 20-μm pore size (NY2002500, Merck Millipore, Billerica, MA) was placed on the bottom of a 10-ml syringe (BD Biosciences, San Jose, CA), followed by stacking of 10 ml Sepharose CL-2B. On top of the SEC column, 2 ml of sample was loaded and fractions of 1 ml eluate were collected. The EV-enriched eluates, being 4–7, were pooled and concentrated approximately 40 times using a centrifugal filter Amicon Ultra-2 10k (Merck Millipore, Billerica, MA). EV-pooled eluates were centrifuged at 3,202*g* using a A-4-62 swinging bucket rotor at 4°C for 10–20 min. Concentrated samples were recovered following the manufactures instructions by centrifugation at 1,000*g* and 4°C for 5 min. Eluates were collected from the flow-through reservoir and resuspended in PBS to a final volume of 100 μl. Samples were next aliquoted in Eppendorf tubes (20 μl) and stored at −80°C until used. The EV obtained from this batch stock were used in the experiments shown. The EV characterization by nanoparticle tracking analysis (NTA) is shown in Supporting Information Figure S1 and described in the Supporting Information Material and Methods.

Fluorescent Staining of EV

EV were stained with PKH67 and separated from contaminants as fully described previously (14). In brief, 10 μl of the isolated reference 4T1 EV (corresponding to a concentration of 1.44 E12 particles/ml as determined by NTA) were stained with PKH67 (Sigma-Aldrich, St Louis, MO), and separated from protein aggregates and free dye by bottom-up density gradient centrifugation in sucrose for 17.30 h at 192,000*g* and 4°C using a SW40 rotor (k-factor 144.5; Beckman Coulter, Fullerton, CA). Twelve fractions of 1 ml were then collected from the top of the gradient and respective densities were determined by refractometry using an Atago Illuminator (Japan). No further SEC was required on these pure EV fractions. For subsequent analysis by flow cytometry, M4T1 EV-PKH67 samples corresponding to a 1.14 g/ml density were diluted 1:20 in PBS (Fig. 4) and further serially diluted to 1:40 and 1:80 in PBS (Supporting Information Fig. S1C,D). MIFlowCyt-EV guidelines (21) were followed whenever applicable (Supporting Information Data S2).

Fluorescence Calibration

For calibration of the fluorecence axis we used fluorescein isothiocyanate (FITC) molecules of equivalent soluble fluorochrome (MESF) beads (custom made, lot MM2307 #131-10; #131-8; #130-6; #130-5; 130-3, BD Biosciences, San Jose, CA). FITC-MESF beads were provided with assigned numbers of MESF for each peak intensity. Briefly, each bead peak population was gated using FlowJo Version 10.5.0 and MFI were obtained (Supporting Information Fig. S2A–C). Next, the

software FCM_{PASS} Version v2.17 was used to perform a least square linear regression analysis and to generate the histogram showing FITC-MESF calibrated axis units (Fig. 4F) (22) (Software is available on http://go.cancer.gov/a/y4ZeFtA).

Data Availability

All EV data of our experiments have been submitted to the EV-TRACK knowledgebase (EV-TRACK ID: EV190050) (23). All flow cytometric data files have been deposited at the Flow Repository (FR-FCM-Z272).

Results

We here tested a combination of differently sized obscuration bars and differently sized pinholes in the optical light path of the FSC detector. With the appropriate pinhole fitted and after careful focusing, the light reaching the detector can be confined to the core of the fluid stream, eliminating the majority of light coming from other directions (Fig. 1). We deployed a matrix in which all possible combinations of five differently sized obscuration bars and six different pinholes were tested in front of the FSC detector. For each combination, the PMT voltages were adjusted to allow the 100-nm fluospheres cluster to reach the exact same mean light scatter and fluorescence values for all measurements. This was done to allow a fair comparison between the specific signals and the background noise in each specific situation. Subsequently, a file without a sample running was recorded to determine the amount of background events for each condition. The electronics of the BD Influx can process up to 200,000 events/s. The closer this rate is reached, the more unreliable the total number of events per measurement will be. All measurements in the range of 200,000 events/s were defined as "too many to count" (TMTC) as indicated by the color gradient in Figure 2. Each measurement was recorded twice; once with a FL threshold at a value of 0.62 and once with a FSC threshold at a value of 0.72. The latter threshold was set slightly higher to avoid the situation of having TMTC in a large number of (sub-optimal) combinations. The number of ungated events collected during 30 s without a sample running was next displayed in a heat map matrix (Fig. 2). Data in red indicate TMTC, whereas all data in orange, yellow, and green fall within the reliable detection range. As expected, the measurements performed with a threshold based on FL display a relatively constant level of background noise for all applied combinations of obscuration bars and pinholes (Fig. 2A). As the changes in configuration only took place on the FSC detector, these data show that the number of fluorescent background events remains unaffected by modification of the FSC optical axis. When a FSC threshold was applied the total number of detected background events was, however, severely affected by the different combinations of obscuration bars and pinholes fitted in the optical axis of the FSC detector (Fig. 2B). The number of background events reduce at increasing sizes of obscuration bars and decreasing pinhole sizes, but counter intuitively at pinhole sizes of 100 µm and smaller the number of background events increases again. It has to be considered that the measurements were normalized. Under each condition in which the pinhole size was decreased or the obscuration bar size was increased, the voltage of the FSC detector had to be increased to reach the given mean scatter and FL values. This indicates that specific signal is reduced as well but to a lesser extent than background light and scatter light from out-of-focus particles. This selective reduction of background light works down to a pinhole size of 200 µm. Below the 200-µm pinhole, the sizes of the smaller pinholes do not allow full passage of the scatter derived from the focused particle and the apparent background becomes visible in these normalized measurements because of increasing voltage settings. Highest voltage applied in this series was 582.6. These effects on the of the number of background events can be explained by the fact that background light is a not-to-be neglected component of the total noise in the signal and is effectively reduced by decreasing pinhole and/or increasing obscuration bar sizes until the combination of a 200-µm pinhole with an 8-mm blocker bar on this BD Influx.

Next, the combinations that resulted in the lowest numbers of background in Figure 2B (FSC threshold) were selected (50-, 100-, and 200-µm pinholes in combination with either a 5-, 8-, or 10-mm obscuration bar) and were recorded again, but now with a reduced FSC threshold value of 0.27 (Fig. 2C). These data show that the combination of an 8-mm blocker bar and a 200-µm pinhole clearly stands out from the other 29 tested combinations regarding the number of background events that are being detected during FSC thresholding.

Since FL threshold in our hands displays the highest signal-to-noise ratio and generates the most reliable results when measuring submicron-sized particles, we next compared the standard configuration (5-mm obscuration bar, 700-µm pinhole), as described in van der Vlist et al. (14) with the optimized configuration (8-mm obscuration bar, 200-µm pinhole) using a FL threshold on 100-nm fluospheres and without a sample running (Fig. 3A–D). When compared to the standard configuration, density dot plots clearly display a reduced number of background noise events within the FSC channel of both the 100-nm fluospheres (Fig. 3A–B) and the measurement without sample running (Fig. 3C,D) when the 8-mm obscuration bar and 200-µm pinhole were fitted.

With the optical background within the FSC channel now effectively being reduced by the bigger obscuration bar and smaller pinhole, we next tested whether the enhanced signal-to-noise ratio also allowed for enhanced detection of 100-nm fluospheres and reduction of noise using FSC thresholding (Fig. 3E–J). While there is a high amount of background noise present within the density dot plots of the backflush and 100-nm fluospheres, when the standard configuration of obscuration bar and pinhole is applied (Fig. 3E,H), the optical background is significantly reduced upon fitting the 8-mm obscuration bar and 200-µm pinhole for both beads and backflush (Fig. 3F,I, respectively). However, since part of the 100-nm fluorescent bead cluster was below the applied threshold of 0.72 when the optimized configuration

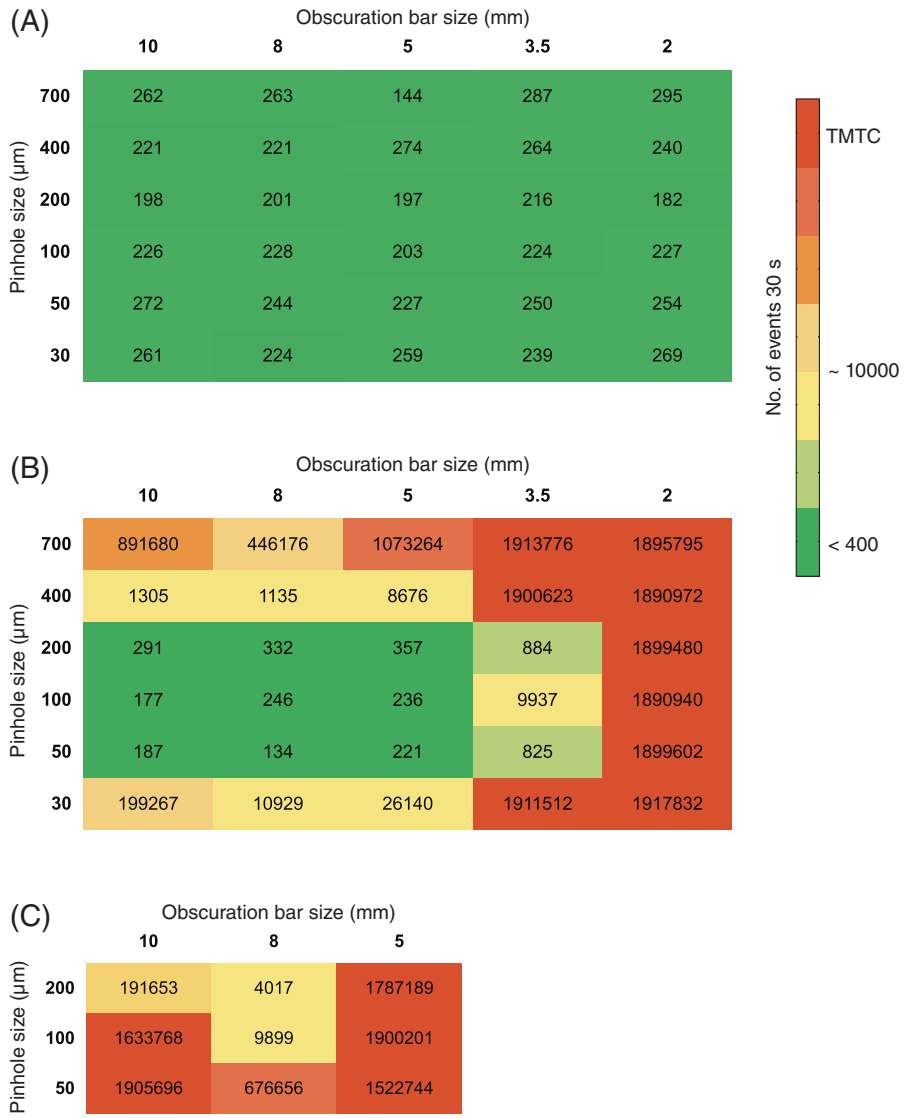

Figure 2. Matrix showing the number of events from a 30 s background measurement. The numbers in each cell represents the number of events under conditions as defined by the size of the obscuration bar (horizontal) and the size of the pinhole (vertical). Panel A shows the results when fluorescence threshold is applied (threshold 0.62). Panel B shows the results for the same configurations as in Panel A but in FSC threshold mode (threshold 0.72). To further enhance configurations with the lowest numbers of events in the FSC threshold mode (50-, 100-, 200-nm pinholes in combination with either a 5-, 8-, or 10-mm obscuration bar), these combinations were recorded again, with a reduced threshold (0.27) as displayed in Panel C. [Color figure can be viewed at wileyonlinelibrary.com]

was fitted (Fig. 3F) a lower threshold (0.27) was applied to resolve the entire bead population (Fig. 3G,J). Although this resulted in more background noise (Fig. 3J), our data show that when a 8-mm obscuration bar and 200-µm pinhole were deployed, the 100-nm polystyrene beads could be clearly resolved from background noise upon FSC thresholding (Fig. 3G) with an acceptable level of background. Taken together, these data thus show that when the optical background is reduced by applying an optimally sized obscuration bar and pinhole in front of the FSC detector, the signal-to-noise ratio of the FSC parameter can be significantly improved for submicron-sized particles.

We have realized the importance of FSC by analysis of virus-containing EV populations that could solely be discriminated from nonvirus-containing EV based on the contribution of FSC (11). Since EV have a comparable size, but a distinctly lower refractive index (RI ≈ 1.4) than polystyrene beads (RI ≈ 1.6), we finally tested the significance of improved background reduction on a biological sample containing EV. Hence, we isolated and characterized an EV sample derived from mouse mammary carcinoma 4T1 cell culture supernatants (M4T1 EV, Supporting Information Fig. S1 and Supporting Information Materials and Methods) and fluorescently stained the EV with the lipophilic generic

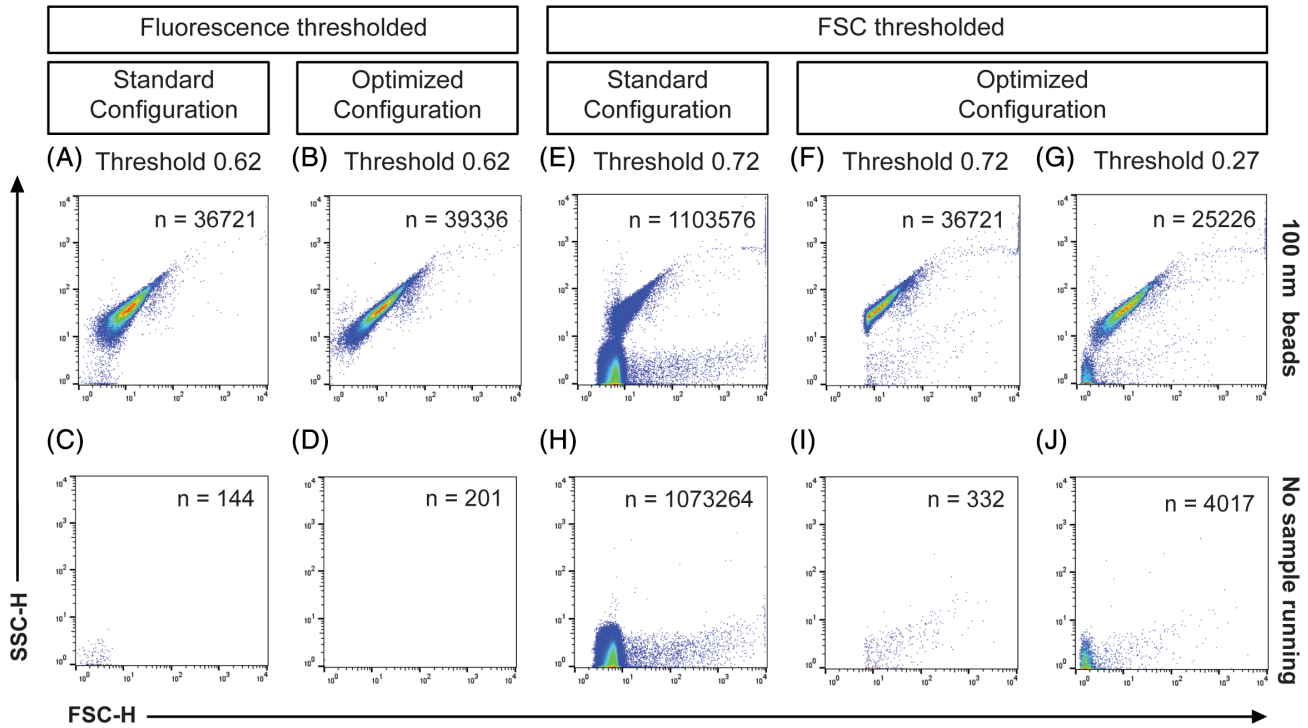

Figure 3. Measurements of 100 nm polystyrene beads in fluorescence (A, B) or FSC (E–G) threshold mode with the respective measurements without sample running (C, D) and (H–J) as background definition. Density plots show a comparison between the standard configuration (5-mm obscuration bar, 700-µm pinhole) and the optimized configuration (8-mm obscuration bar, 200-µm pinhole). [Color figure can be viewed at wileyonlinelibrary.com]

membrane dye PKH67. Next we compared the standard configuration and optimized obscuration bar-pinhole configuration by measuring these PKH67-stained M4T1 derived EV using a FL or FSC thresholding (Fig. 4). When the standard configuration (Fig. 4A) is compared to the optimized configuration (Fig. 4B) during FL thresholding a clear improvement is observed, as noise events overlapping the EV move toward the FSC baseline, thereby allowing a noise-free display of the EV cluster (Fig. 4B). The combination of an 8-mm obscuration bar and 200-µm pinhole thereby allowed a better separation between fluorescently stained EV and noise that appeared above the FL threshold. Using FSC thresholding in the standard configuration (Fig. 4C) the threshold had to be set at 0.72 to avoid an unacceptable high number of background counts. Because of this threshold level, a large part of the EV remains below the FSC threshold level and the EV cluster in the density plot appears to be clipped. This becomes even more evident when using this threshold setting in the optimized configuration (Fig. 4D). However, for this highly purified EV sample the optimized configuration allowed to resolve the vast majority of EV after FSC threshold was reduced to a value of 0.27 (Fig. 4E). Figure 4F shows the histogram of the EV plotted with a FITC calibrated axis to give an indication of the median PKH67 FL intensity of the EV population in standard units of MESF. The majority of the EV population has a FL intensity equivalent to approximately 300 FITC-MESF when measured on this instrument. The FL threshold value of 0.62 on this BD Influx corresponds to an equivalent of 100 FITC-MESF, which corresponds with the lower end of the population in the histogram. The bar graph (Fig. 4G) shows the number of events measured for the same sample with the optimized configuration in a quantitative manner. The background number of events derived from clean PBS measurements in identical configurations was subtracted to allow a fair comparison. While measurements performed in the optimized configuration with high FSC threshold (0.72) show lower numbers of events as compared to FL thresholding, the measurements performed with low FSC threshold (0.27) clearly show the improvement in the detection of EV, thereby allowing for the visualization of comparable numbers of EV to those observed in the FL thresholded measurements.

Discussion

The signal-to-noise ratio on a flow cytometer greatly determines its resolution and sensitivity and this becomes specifically evident when measuring the dim signals transmitted by submicron-sized particles. One prominent source of background noise is optical background caused by laser stray light, and particularly light scatter parameters are vulnerable to the optical background caused by stray light of the thresholding

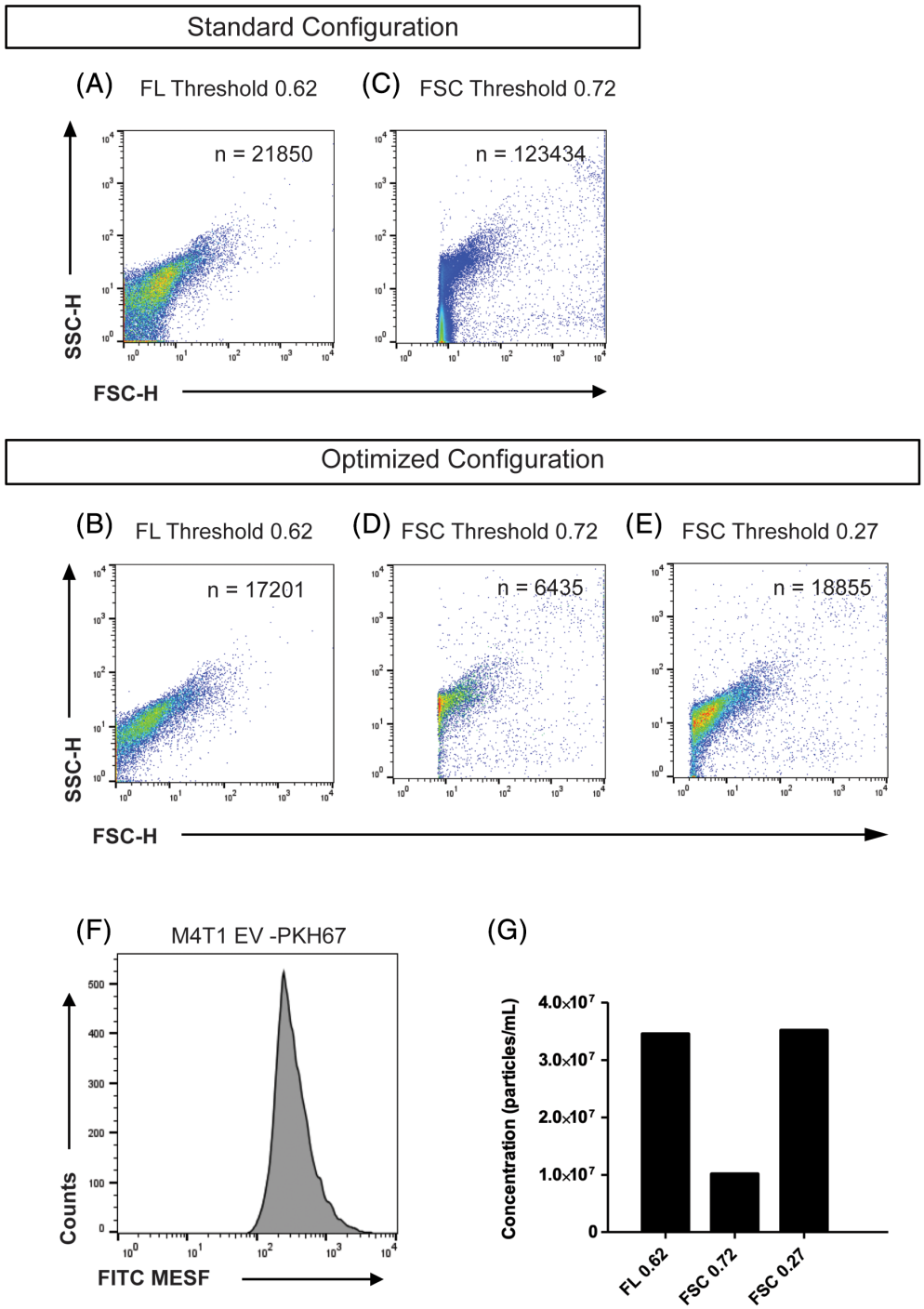

Figure 4. Density plots showing measurements of PKH67-stained M4T1 derived EV in a comparison between the standard configuration of the FSC detector optics (5-mm obscuration bar, 700-μm pinhole, A, C) and the optimized configuration (8-mm obscuration bar, 200-μm pinhole, B, D, E). Panels A and B are in fluorescence thresholding mode. Panels C–E are in FSC thresholding mode. F Histogram displaying FITC-MESF calibrated axis for PKH67 stained M4T1 EV, same as shown in Panel B. (G) Bar graph displaying concentration measured with the optimized configuration in fluorescence thresholding mode (threshold value of 0.62) and FSC thresholding mode (threshold values of 0.72 and 0.27) as indicated. Concentration was corrected for dilution, flow rate, time measurement and the number of events detected in PBS background controls (which total numbers of events were 185, 1,456, and 1,522 respectively). [Color figure can be viewed at wileyonlinelibrary.com]

laser. The overarching aim of this study was to improve the information obtained from the FSC detector during the analysis of submicron-sized particles. To do so, we have tested a series of differently sized obscuration bars and pinholes on the FSC detection unit of a BD Influx flow cytometer that was previously optimized for the detection of submicron-sized particles (14). The main effective principle in our configuration is confocal detection. For every particle out of the focal spot, the scattering light will be reduced because it is not perfectly focused on the pinhole. This reduction also applies for optical background caused by ambient light and laser stray light that is coming in from any aberrant direction. The purpose was to find an optimal combination of obscuration bar and pinhole to allow a better separation between signal and background when measuring small and dim particles, such as EV. With the various combinations of obscuration bars and pinholes we have tested, absolute values of the signals of interest were going down with an increase in obscuration bar size or a decrease in pinhole size. Background signals reduce concurrently, but when an optimized configuration using a combination of an 8-mm obscuration bar and 200-μm pinhole was fitted, the specific signal improved relative to the background (Fig. 2). With a FL threshold set at 0.62, reduction on background was such that we could separate 100-nm polystyrene beads from noise in the FSC channel, something that was not possible when the standard configuration (5-mm obscuration bar and 700-μm pinhole) was used (Fig. 3A–D). Moreover, when the optimized configuration was applied even FSC thresholded measurements of 100-nm polystyrene beads could be performed while maintaining acceptable background levels (Fig. 3G,J). Importantly, with the optimized configuration we were not only able to diminish noise during fluorescent thresholded analysis of purified fluorescently stained EV (Fig. 4B), but we even managed to improve detection of these EV (mean size: 139.8 nm as determined by NTA and shown in Supporting Information Fig. S1A) by performing FSC-thresholded measurements (Fig. 4E). Although we have shown that there is an optimal obscuration bar/pinhole combination, the semi-quantitative analysis presented in this study does not address the details of collection efficiency and the description in terms of the Fourier optical system. Future work is required to confirm the configuration effects in detail with regards to these points.

Despite the fact that these improvements allow for the detection of purified EV on the basis of FSC, biological samples are likely to contain massive amounts of non-EV-related material (i.e., insoluble protein complexes, lipoprotein particles and salt crystals) that scatters light and that can interfere with the detection of EV of interest (24, 25). Hence, to allow acquisition of EV in complex biological samples using these optimized settings, thorough EV purification still remains mandatory for a clear-cut distinction between EV, optical noise and events of noninterest by FSC thresholding. Performing a generic fluorescent staining strategy can aid to exclude non-EV-related signals from the sample and can help to resolve smaller-sized EV from background noise. In this study we have used PKH67 stained EV that were characterized to have an approximate median FL intensity of an equivalent of 300 FITC-MESF (Fig. 4F). There are, however, two points that need to be considered here. Firstly, plotting non-FITC-labeled EV on a FITC calibrated axis is dependent on the type and quality of the band-pass filter used, as samples might turn out to have different values when measured on other instruments. Intercomparison of instruments therefor requires that spectrally unmatched fluorophore-related correction factors should be defined and applied (26). Secondly, MESF values in the very dim area are obtained by extrapolation of the regression line in the log–log converted calibration plot. This relies heavily on the linearity of the measurements and the subsequent fit of the regression line. Small deviations within the fluorochrome range of the calibration beads will have substantial effects in the area where EV-related FL can be expected. The average of 300 FITC-MESF for PKH67-labeled EV in Figure 4F therefore has to be considered as the best possible approximation in standardized units, using currently available bright FITC-calibration beads, which applies to the specific filter settings on the used BD Influx.

With orientation of the collection angle and the scattering effects of submicron particles in mind, SSC remains the better scatter parameter to resolve submicron-sized particles like EV on the majority of conventional flow cytometers (27) (28). It, however, cannot be ignored that the FSC detection unit on conventional flow cytometers is often designed with cost-efficiency in mind, not resolution. For the analysis of submicron-sized particles, the current design of most FSC detection units is thus insufficient and data considering FSC are largely ignored and uninterpretable. In the current study we show that the signal-to-noise ratio on the FSC detector can be significantly improved using simple technical modifications on a BD Influx jet-in-air flow sorter. We would like to stress that our study is meant to create awareness that optical background is a serious component influencing the detection limits of flow cytometers. As our findings allow improved FSC detection of submicron-sized particles, these considerations might be put into effect in dedicated small particle instruments that are brought on the market in the future.

Acknowledgments

The authors would like to thank Prof. An Hendrix (Laboratory of Experimental Cancer Research, Ghent University, Belgium) for the possibility to prepare and analyze M4T1-derived EV in her lab and Dr. Joshua A. Welsh (National Cancer Institute, Bethesda, MD) for helpful discussion. FITC-MESF beads were kindly provided as a gift by BD Biosciences (custom beads, prepared by Dr. Majid Mehrpouyan). E. L. A. is supported by the European Union's Horizon 2020 research and innovation program under the Marie Skłodowska-Curie grant agreement no. 722148. S. F. W. M. L. was supported by the Dutch Technology Foundation STW (Perspectief Program Cancer ID, project 14191), which is part of the Netherlands Organization for Scientific Research (NWO), and which is partly funded by the Ministry of Economic Affairs.

Conflict of Interests

During this study, the Wauben Research Group, Utrecht University, Faculty of Veterinary Medicine, Department of Biochemistry and Cell Biology, had a collaborative research agreement with BD Biosciences Europe, Erembodegem, Belgium.

Literature Cited

1. van Niel G, D'Angelo G, Raposo G. Shedding light on the cell biology of extracellular vesicles. Nat Rev Mol Cell Biol 2018;19(4):213–228.
2. Nolan JP. Flow cytometry of extracellular vesicles: Potential, pitfalls, and prospects. Current protocols in cytometry. 2015;73:13.4.1–13.4.6.
3. Lacroix R, Robert S, Poncelet P, Kasthuri RS, Key NS, Dignat-George F, ISTH SSC Workshop. Standardization of platelet-derived microparticle enumeration by flow cytometry with calibrated beads: Results of the international society on thrombosis and haemostasis SSC collaborative workshop. J Thromb Haemost 2010;8(11): 2571–2574.
4. Chandler WL, Yeung W, Tait JF. A new microparticle size calibration standard for use in measuring smaller microparticles using a new flow cytometer. J Thromb Haemost 2011;9(6):1216–1224.
5. Robert S, Poncelet P, Lacroix R, Raoult D, Dignat-George F. More on: Calibration for the measurement of microparticles: Value of calibrated polystyrene beads for flow cytometry-based sizing of biological microparticles. J Thromb Haemost 2011;9 (8):1676–1678. author reply 81–2.
6. Mullier F, Bailly N, Chatelain C, Dogne JM, Chatelain B. More on: Calibration for the measurement of microparticles: Needs, interests, and limitations of calibrated polystyrene beads for flow cytometry-based quantification of biological microparticles. J Thromb Haemost 2011;9(8):1679–1681. author reply 81–2.
7. Zhu S, Ma L, Wang S, Chen C, Zhang W, Yang L, Hang W, Nolan JP, Wu L, Yan X. Light-scattering detection below the level of single fluorescent molecules for high-resolution characterization of functional nanoparticles. ACS Nano 2014;8(10): 10998–100006.
8. Steen HB. Flow cytometer for measurement of the light scattering of viral and other submicroscopic particles. Cytomet A J Int Soc Anal Cytol 2004;57(2):94–99.
9. Yang L, Zhu S, Hang W, Wu L, Yan X. Development of an ultrasensitive dual-channel flow cytometer for the individual analysis of nanosized particles and biomolecules. Anal Chem 2009;81(7):2555–2563.
10. Zucker RM, Ortenzio JN, Boyes WK. Characterization, detection, and counting of metal nanoparticles using flow cytometry. Cytomet A J Int Soc Anal Cytol 2016;89 (2):169–183.
11. van der Grein SG, Defourny KAY, Rabouw HH, Galiveti CR, Langereis MA, Wauben MHM, Arkesteijn GJA, van Kuppeveld FJM, Nolte-'t Hoen ENM. Picornavirus infection induces temporal release of multiple extracellular vesicle subsets that differ in molecular composition and infectious potential. PLoS Pathogen 2019; 15(2):e1007594.
12. Arraud N, Gounou C, Turpin D, Brisson AR. Fluorescence triggering: A general strategy for enumerating and phenotyping extracellular vesicles by flow cytometry. Cytomet A J Int Soc Anal Cytol 2016;89(2):184–195.
13. Nolte-'t Hoen EN, van der Vlist EJ, Aalberts M, Mertens HC, Bosch BJ, Bartelink W, Mastrobattista E, van Gaal EV, Stoorvogel W, Arkesteijn GJ, et al. Quantitative and qualitative flow cytometric analysis of nanosized cell-derived membrane vesicles. Nanomed Nanotech Biol Med 2012;8(5):712–720.
14. van der Vlist EJ, Nolte-'t Hoen EN, Stoorvogel W, Arkesteijn GJ, Wauben MH. Fluorescent labeling of nano-sized vesicles released by cells and subsequent quantitative and qualitative analysis by high-resolution flow cytometry. Nat Protocol 2012;7 (7):1311–1326.
15. Groot Kormelink T, Arkesteijn GJ, Nauwelaers FA, van den Engh G, Nolte-'t Hoen EN, Wauben MH. Prerequisites for the analysis and sorting of extracellular vesicle subpopulations by high-resolution flow cytometry. Cytomet A J Int Soc Anal Cytol 2016;89(2):135–147.
16. Libregts SFWM, Arkesteijn GJA, Nemeth A, Nolte-'t Hoen ENM, Wauben MHM. Flow cytometric analysis of extracellular vesicle subsets in plasma: Impact of swarm by particles of non-interest. J Thromb Haemost 2018;16(7):1423–1436.
17. Wood JC, Hoffman RA. Evaluating fluorescence sensitivity on flow cytometers: An overview. Cytometry 1998;33(2):256–259.
18. Blume P. A spectrophotometric method for determining the stream sample core diameter of a flow cytometer. Cytometry 1989;10(3):351–353.
19. Geeurickx E, Tulkens J, Dhondt B, Van Deun J, Lippens L, Vergauwen G, Heyrman E, De Sutter D, Gevaert K, Impens F, et al. The generation and use of recombinant extracellular vesicles as biological reference material. Nat Commun 2019;10(1):3288. https://doi.org/10.1038/s41467-019-11182-0.
20. Vergauwen G, Dhondt B, Van Deun J, De Smedt E, Berx G, Timmerman E, Gevaert K, Miinalainen I, Cocquyt V, Braems G, et al. Confounding factors of ultrafiltration and protein analysis in extracellular vesicle research. Sci Rep 2017;7(1): 2704. https://doi.org/10.1038/s41598-017-02599-y.
21. Welsh JA, Van Der Pol E, Arkesteijn GJA, Bremer M, Brisson A, Coumans F, Dignat-George F, Duggan E, Ghiran I, Giebel B, et al. MIFlowCyt-EV: A framework for standardized reporting of extracellular vesicle flow cytometry experiments. J Extracell Vesicles 2020;9(1):1713526.
22. Welsh JA, Horak P, Wilkinson JS, Ford VJ, Jones JC, Smith D, Holloway JA, Englyst NA. FCMPASS software aids extracellular vesicle light scatter standardization. Cytomet A 2019;28(10):1002.
23. EV-TRACK Consortium, Van Deun J, Mestdagh P, Agostinis P, Akay O, Anand S, Anckaert J, Martinez ZA, Baetens T, Beghein E, et al. EV-TRACK: Transparent reporting and centralizing knowledge in extracellular vesicle research. Nat Methods 2017;14(3):228–232.
24. Yuana Y, Levels J, Grootemaat A, Sturk A, Nieuwland R. Co-isolation of extracellular vesicles and high-density lipoproteins using density gradient ultracentrifugation. J Extracellular Vesicles 2014;3(1):23262. https://doi.org/10.3402/jev.v3.23262.
25. Sodar BW, Kittel A, Paloczi K, Vukman KV, Osteikoetxea X, Szabo-Taylor K, Németh A, Sperlágh B, Baranyai T, Giricz Z, et al. Low-density lipoprotein mimics blood plasma-derived exosomes and microvesicles during isolation and detection. Sci Rep 2016;6:24316.
26. Hoffman RA, Wang L, Bigos M, Nolan JP. NIST/ISAC standardization study: Variability in assignment of intensity values to fluorescence standard beads and in cross calibration of standard beads to hard dyed beads. Cytomet A 2012; 81(9):785–796.
27. de Rond L, van der Pol E, Hau CM, Varga Z, Sturk A, van Leeuwen TG, Nieuwland R, Coumans FAW. Comparison of generic fluorescent markers for detection of extracellular vesicles by flow cytometry. Clin Chem 2018;64(4): 680–689.
28. McVey MJ, Spring CM, Kuebler WM. Improved resolution in extracellular vesicle populations using 405 instead of 488 nm side scatter. J Extracell Vesicles 2018; 7(1):1454776.